Journal of Materials Science: Materials in Electronics (2019) 30:12545–12554
https://doi.org/10.1007/s10854-019-01615-3

Growth, structure, optical and optoelectrical characterizations of the Cu_2NiSnS_4 thin films synthesized by spray pyrolysis technique

H. I. Elsaeedy[1]

Received: 24 February 2019 / Accepted: 29 May 2019 / Published online: 22 June 2019

Abstract

Earth-abundant Kesterite materials are very important to fabricate low-cost solar cells. Here, good quality Cu_2NiSnS_4 (CNSS) thin films were successively manufactured on a glass substrate at 350 °C using a simple spray pyrolysis system. The structural characterization of the sprayed Cu_2NiSnS_4 thin films was examined by the FE-SEM and XRD techniques. X-ray diffraction patterns indicate that the sprayed Cu_2NiSnS_4 films are single phase and having polycrystalline structure. The elemental composition analysis of the sprayed Cu_2NiSnS_4 thin films confirmed that the Cu_2NiSnS_4 film is near stoichiometric in compound. Our optical observations indicate that the refractive index (n) of the sprayed Cu_2NiSnS_4 films was increased by increasing the film thickness. Moreover, the sprayed Cu_2NiSnS_4 films exhibit a direct optical transition and the magnitudes of the energy gap have been decreased from 1.28 to 1.14 eV with the increase of thickness. The optoelectrical parameters of the Cu_2NiSnS_4 films, like optical conductivity, optical mobility, optical resistivity, optical carrier concentration and relaxation time were estimated with different thickness. Additionally, the nonlinear optical parameters of the Cu_2NiSnS_4 films were estimated. The fabricated CNSS/n-Si heterojunction achieved a conversion efficiency of 11.34%.

1 Introduction

Kesterite thin films of the structure Cu_2-M-Sn-X_4 (M = Zn, Cd, Mn, Co and X = S, Se) attached a great deal of attention in the current articles owing to they have a high absorption coefficient, a promising energy gap, the low-cost element and high earth abundant of all elements [1–4]. The Cu_2ZnSnS_4 (CZTS) is one of the important Kesterites that utilized as absorber layer in the solar cell. CZTS thin film solar cell was fabricated via vacuum and non-vacuum procedures. The efficiency of the CZTS solar cell reaches to about 9.6% by thermal evaporation process [5] and reaches to 5.1% by spray pyrolysis technique [6]. The substitution of Zinc in the CZTS thin film with other transition metals like Nickel, cobalt and iron will produce some new materials like Cu_2NiSnS_4, Cu_2CoSnS_4, Cu_2FeSnS_4 suitable for the PV devices [7].

Cu_2NiSnS_4 has a similar structure to the Cu_2ZnSnS_4 material. The Cu_2NiSnS_4 is an important p-type Kesterite material which has a high absorption coefficient (large than 10^4 cm^{-1}) and a promising band gap in the 1.14–1.3 eV range [8]. Several preparation methods were utilized to manufacture the Cu_2NiSnS_4 thin films like solvothermal method [9], hydrothermal [10], hot injection [11], spin coating method [12], electrodeposition [13], and dip coating [14] techniques.

The previous articles on the Cu_2NiSnS_4 films were focused on some linear optical properties as the band gap and the absorption coefficient. Chen et al. [13] shows that the Cu_2NiSnS_4 thin films exhibit a high absorption coefficient and a suitable band gap. Krishnaiah et al. [14] demonstrates that the magnitudes of energy gap were decreased with increasing the dipping time. On the other hand, the studies on the other optical parameters of the Cu_2NiSnS_4 thin films like, refractive index, extinction coefficient, optoelectrical parameters and nonlinear optical parameters were not presented in the articles so, in the present work, special focus is set on the optoelectrical parameters, linear and nonlinear optical parameters of the Cu_2NiSnS_4 films.

✉ H. I. Elsaeedy
halsayede@kku.edu.sa

[1] Advanced Functional Materials & Optoelectronic Laboratory (AFMOL), Department of Physics, Faculty of Science, King Khalid University, P.O. Box 9004, Abha, Saudi Arabia

2 Experimental section

2.1 Thin film synthesis

High quality Cu_2NiSnS_4 films were fabricated on cleaned glass substrates via an inexpensive spray pyrolysis deposition method 350 °C. The Cu_2NiSnS_4 precursor solution composed of 0.1 M copper nitrate dehydrate, 0.05 M nickel nitrate dehydrate, 0.05 M stannic chloride dehydrate and 0.2 M thiourea. A mixture of methanol to water ratio of 1:2 ml has been used for solution preparation. The pH of the solution set at 9. The final Cu_2NiSnS_4 solution was sprayed into a heated glass substrate held at 350 °C. The spray process occurred at different spray times 10, 20, 30 and 40 min. A digital temperature controller joined with a thermocouple was used to control the substrate temperature. After the preparation, thin films were cooled at ambient temperature. The sprayed Cu_2NiSnS_4 films were uniform and adherent to the substrates.

2.2 Fabrication of Ag/n-Si/CNSS/Au heterojunction

Firstly, the n-type single crystal silicon wafer subjected to etching processing using a CP_4 solution consists of 5 HNO_3: 3 HF: 3 CH_3COOH to clear any oxide layer from the surface of the silicon wafer, thereafter the silicon wafer was cleaned with ethyl alcohol and deionized water respectively. Then, Ag electrode has been deposited onto the back surface of the Si substrate by thermal evaporation technique to form the bottom ohmic contacts. The CNSS thin film of thickness 461 nm was sprayed on the top of the n-Si wafer by spray pyrolysis method. The top ohmic electrode was formed by evaporating of Au metal onto CNSS films. The Ag/n-Si/CNSS/Au heterojunction device has been represented in Fig. 1.

2.3 Characterization of the Cu_2NiSnS_4 thin films

The thickness of the sprayed Cu_2NiSnS_4 thin films was estimated by using alpha step D 500 stylus profilometer. The structural characterization of the Cu_2NiSnS_4 thin films was analyzed by Philips X' pert diffractometer with CuKα radiation (λ = 1.540 Å). The surface morphology of the Cu_2NiSnS_4 thin films were studied by field emission scanning electron microscope (FE-SEM) type (type FESEM, Quanta FEG 250, and FEI, USA). The optical, optoelectrical and nonlinear optical properties of the Cu_2NiSnS_4 thin films were evaluated by measuring both of transmittance and reflectance for the Cu_2NiSnS_4 thin films in the range of 400–2500 nm via spectrophotometer (type JASCO Corp., V-570). The current–voltage characterization of the Ag/n-Si/CNSS/Au heterojunction was recorded by high impedance electrometers (Type Keithley 614). A halogen lamp with intensity of 100 mW/cm^2 has been used to illuminate the Ag/n-Si/CNSS/Au heterojunction.

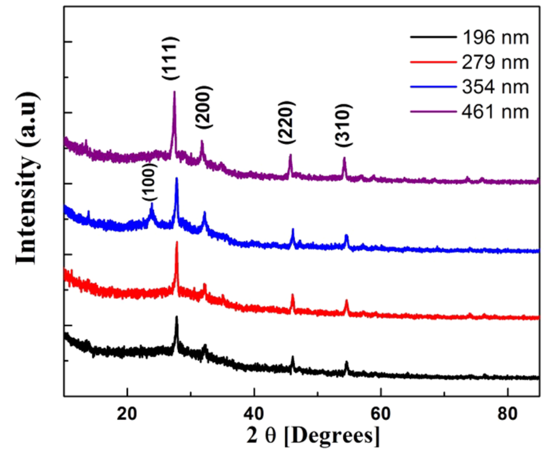

Fig. 1 X-ray diffraction spectra for the Cu_2NiSnS_4 thin films

3 Results and discussion

3.1 Structural analysis

3.1.1 XRD diffraction

Figure 1 represents the results of X-ray diffraction patterns for the Cu_2NiSnS_4 films fabricated at various thicknesses 196 nm, 297 nm, 354 nm and 461 nm. As illustrated in the figure, the presence of sharp peaks confirms the polycrystalline nature of the Cu_2NiSnS_4 thin films. It is clear that the Cu_2NiSnS_4 films are single phase with a cubic structure, which confirmed by good coincidence of *d*–values of observed peaks with Cu_2NiSnS_4 phase in Standard JCPDS file no. 260552, as well the absence of any extra planes that reveal the existence of any secondary phases. The presence of (100) peak for the Cu_2NiSnS_4 film of thickness 354 nm was related to Cu_2NiSnS_4 and this peak could be attributed to the presence of disorder in the hot plate temperatures during the film deposition.

The interplanar spacing d hkl of the given Miller indices h, k and l magnitudes of the Cu_2NiSnS_4 thin films were evaluated via Bragg's law [15]:

$$2d_{hkl}\sin\theta = n\lambda, \tag{1}$$

where n represents the order of diffraction (n = 1) and λ is the wavelength of X-ray. The lattice parameters of the tetragonal structure of the sprayed Cu_2NiSnS_4 thin films were evaluated from the (111) plane using the following relation [16]:

Table 1 The structure parameters for the sprayed Cu_2NiSnS_4 thin films

Film thickness (nm)	D (nm)	$\varepsilon \times 10^{-3}$	$\delta \times 10^{-4}$ (nm)$^{-3}$
196	38.54	9.39	0.673
279	41.92	8.63	0.569
354	45.78	7.91	0.477
461	49.13	7.36	0.414

$$d_{hkl} = \frac{a}{\sqrt[2]{h^2 + k^2 + l^2}} \tag{2}$$

The estimated values of the unit cell volume and the lattice parameters of the sprayed Cu_2NiSnS_4 thin films are recorded in Table 1 and they are in agreement with the JCPDS magnitudes.

The magnitudes of the grain sizes (D), the lattice strain (ε) and the dislocation density (δ) of the sprayed Cu_2NiSnS_4 thin films were calculated by the presented formulas [17–19]:

$$D = \frac{K\lambda}{\beta \cos(\theta)} \tag{3}$$

$$\varepsilon = \frac{\beta cos(\theta)}{4} \tag{4}$$

$$\delta = \frac{1}{D^2} \tag{5}$$

where β represents the full-width at half maximum of the peak (in radian) and θ represents the corresponding Bragg's diffraction angle at the peak position, λ represents the X-ray wavelength (λ = 1.540 Å).

The calculated values of the dislocation density (δ), the lattice strain (ε) and the grain size (D) of the sprayed Cu_2NiSnS_4 thin films were noted in Table 1. It is observed from Table 1 that the increase of the film thickness is attended with an increase in the grain size D and decrease in the lattice strain , and the dislocation density . The dependence of the crystallites size (*D*) and the strain (ε) on the film thickness for the Cu_2NiSnS_4 films were presented in Fig. 2. By increasing the film thickness the crystallites size (*D*) increases and the strain (ε) decreases.

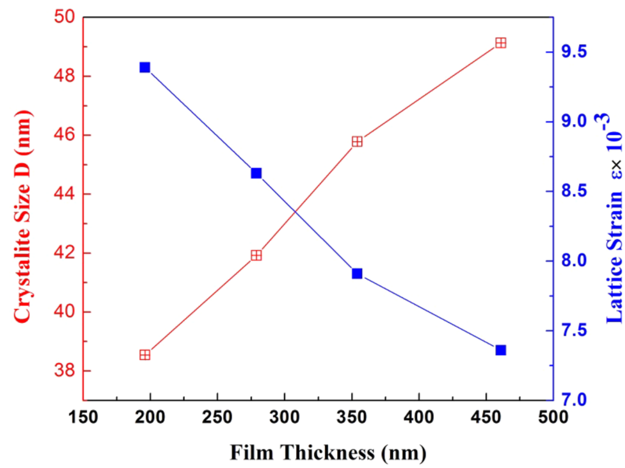

Fig. 2 The crystallite size and lattice strain as a function of the Cu_2NiSnS_4 film thickness

3.1.2 Field emission scanning electron microscope (FE-SEM)

The microstructural of the Cu_2NiSnS_4 thin films has been investigated via field emission scanning electron microscope (FE-SEM). The FE-SEM photograph of the Cu_2NiSnS_4 thin film of thickness 461 nm displays that the film consists of a spherical grains and surface of the film seems to be uniform and homogenous. The EDX pattern of the Cu_2NiSnS_4 thin film of thickness 461 nm approves the presence of copper, nickel, tin and sulfur. The atomic ratio of Cu, Ni, Sn and S in the Cu_2NiSnS_4 thin film is near 2:1:1:4 so the Cu_2NiSnS_4 thin films are near stoichiometric in composition (Fig. 3).

3.2 Linear optical properties

3.2.1 Transmittance and reflectance analysis

The spectral spreading of optical reflectance and transmittance of the sprayed Cu_2NiSnS_4 films of thickness 196 nm, 297 nm, 354 nm and 461 nm as a function of wavelength was represented in Fig. 4a and b. From these curves, the reflectance values increase with the increasing the thickness while the transmittance values decrease with the increasing the film thickness of the sprayed Cu_2NiSnS_4 films.

3.2.2 Absorption coefficient and optical band gap analysis

The absorption coefficient (α) of the Cu_2NiSnS_4 films was calculates via the following expression [20]:

$$\alpha = \frac{1}{t} ln \left[\frac{(1-R)^2}{2T} + \left(\frac{(1-R)^4}{4T^2} + R^2 \right)^{1/2} \right] \tag{6}$$

where t represents the value of film thickness and K represents the extinction coefficient of the Cu_2NiSnS_4 thin films.

The absorption coefficient, α of the Cu_2NiSnS_4 thin films was presented in Fig. 5a. It is appeared from this plot that the

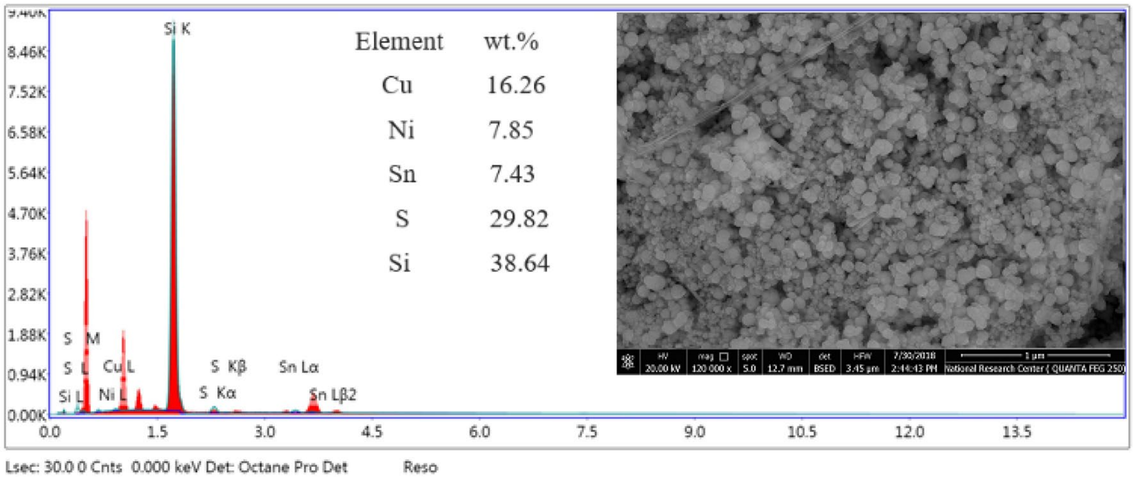

Fig. 3 FE-SEM micrographs and EDX analysis of the Cu_2NiSnS_4 thin film with thickness 461 nm

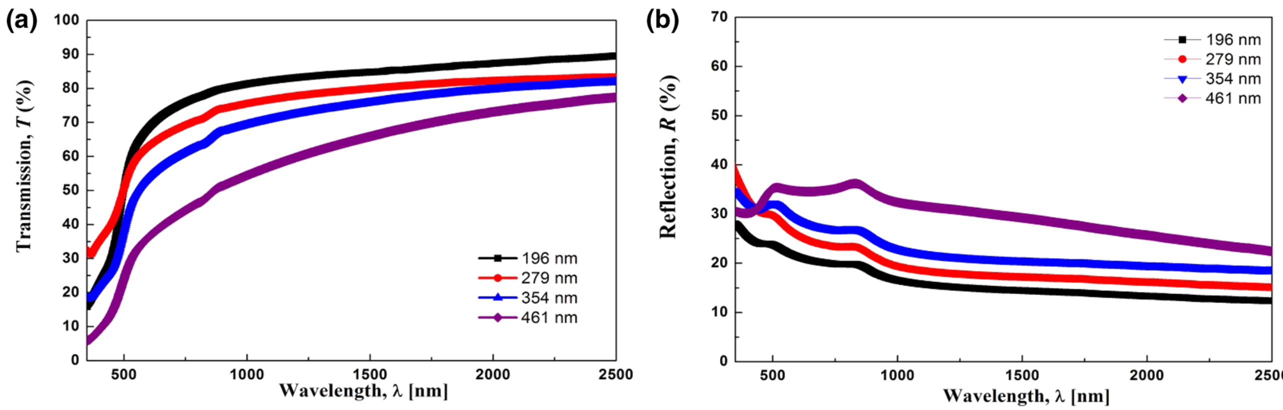

Fig. 4 **a** The transmittance spectra of the sprayed Cu_2NiSnS_4 films under investigation and **b** the reflectance spectra of the sprayed Cu_2NiSnS_4 films

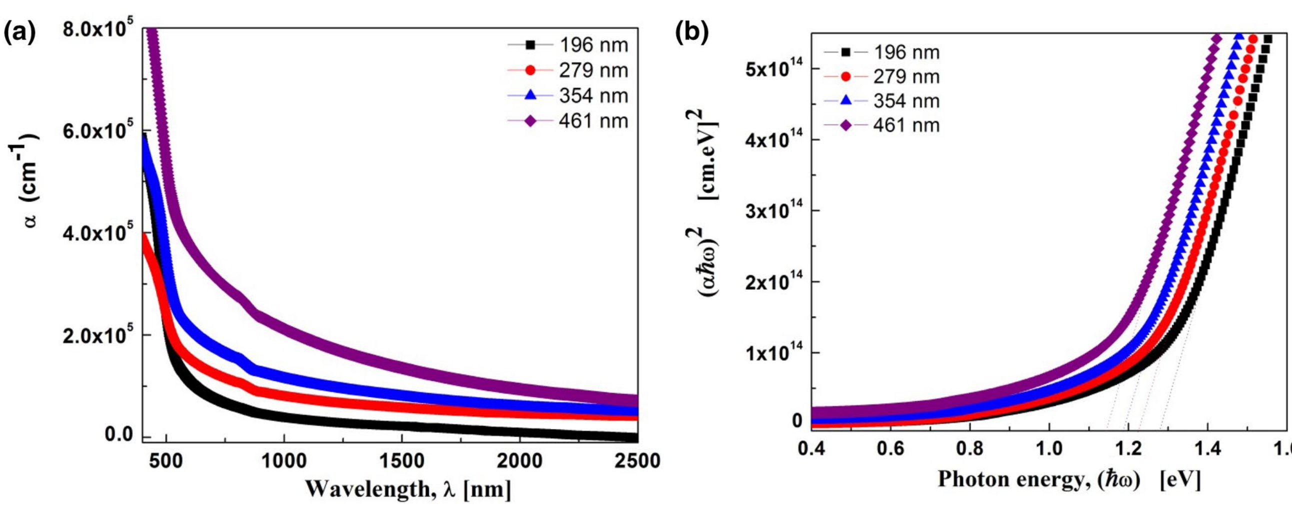

Fig. 5 **a** The absorption coefficient as a function of wavelength for the Cu_2NiSnS_4 thin films, **b** plot of $(\alpha h\nu)^2$ versus the photon energy $h\nu$ for the Cu_2NiSnS_4 thin films

Table 2 The optoelectrical and nonlinear optical parameters for the Cu_2NiSnS_4 films

Film thickness (nm)	E_g^{dir} (eV)	ε_L	N_{opt} ($\times 10^{14}$)	τ ($\times 10^{-26}$)	μ_{opt} ($\times 10^{-14}$)	ρ_{opt} ($\times 10^{18}$)	$^{(3)}$ ($\times 10^{-12}$) [esu]	n_2 ($\times 10^{-11}$) [esu]
196	1.28	3.36	33.17	6.18	4.65	7.43	5.89	0.98
279	1.22	3.1	33.98	5.45	3.79	7.17	7.87	6.97
354	1.19	2.81	35.74	4.76	3.24	4.03	10.31	12.56
461	1.14	2.47	36.67	4.48	2.98	3.71	11.48	14.24

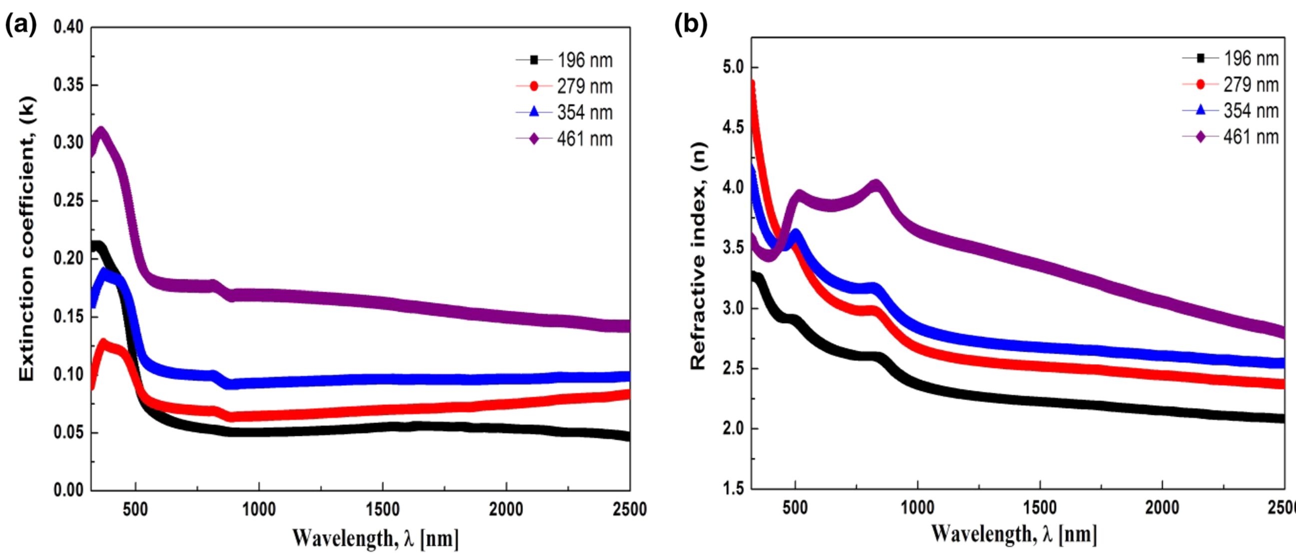

Fig. 6 **a** The extinction coefficient as a function of wavelength for the sprayed Cu_2NiSnS_4 films, **b** the refractive index as a function of wavelength for the sprayed Cu_2NiSnS_4 films under study

absorption coefficient of the Cu_2NiSnS_4 films was decreased as the wavelength increase and increase with increasing the thickness of the Cu_2NiSnS_4 films.

The relation between the absorption coefficient (α) and incident photon energy ($h\upsilon$) in the high absorption region of semiconductor can be used to evaluate the kind of optical band transition relating to Tauc's formula [21]:

$$\alpha h\nu = B\left(h\nu - E_g\right)^n \tag{7}$$

where $h\upsilon$ represents the photon energy, E_g represents the optical band gap, B is complex parameter depending on temperature and photon energy and n is a number determines the type of optical transition process. The magnitudes of n are 1/2, 2, 3/2 and 3 for a direct allowed, indirect allowed, direct forbidden and indirect forbidden transitions, respectively. It was found that the best linear fit for n values were at n equal 1/2, which reveal a direct optical transition. In this study, the value of $n=2$ did not give any linear relation. The values of $(\alpha h\nu)^2$ as a function of the photon energy ($h\nu$) for the Cu_2NiSnS_4 thin films is represented in Fig. 5b. The plot gave a straight line and the value of band gap is obtained by extend this straight line to intercept x-axis at zero absorption. The values of a direct energy gap of the Cu_2NiSnS_4 thin films were listed in Table 2. It can observe from this table that the evaluated direct energy gap were decreased from 1.28 to 1.14 eV by increasing the thickness of the Cu_2NiSnS_4 films this behavior is attributed to many factors, like the increase of grain size, increase of disorders and the variations in barrier height at the grain boundaries through increasing thickness of the sprayed Cu_2NiSnS_4 films [22].

3.2.3 Extinction coefficient and refractive index analysis

For evaluating the magnitudes of the extinction coefficient K of the Cu_2NiSnS_4 thin films we have used the following expression [23]:

$$k = \frac{\alpha\lambda}{4\pi}. \tag{8}$$

The variation of the extinction coefficient of the sprayed Cu_2NiSnS_4 thin films with the wavelength was illustrated in Fig. 6a. It can observe from figure that the magnitudes of

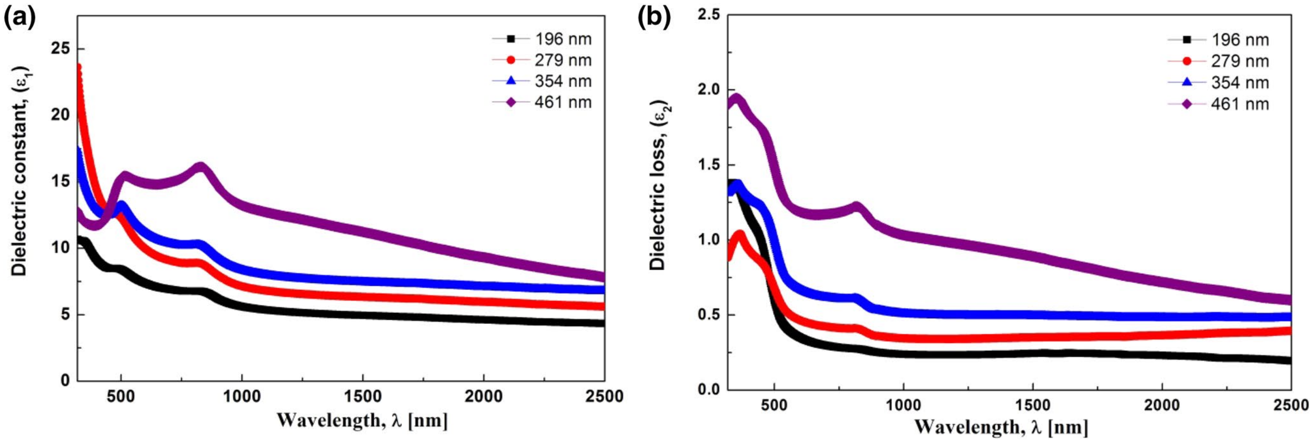

Fig. 7 **a** The variation of the real dielectric constant as a function of wavelength for the sprayed Cu_2NiSnS_4 films, **b** the variation of the imaginary dielectric constant as a function of wavelength for the sprayed Cu_2NiSnS_4 film

the extinction coefficient K were increased with increasing the thickness of the Cu_2NiSnS_4 films and decreases with the increase in wavelength K.

The refractive index (n) of the sprayed Cu_2NiSnS_4 thin films was evaluated by the Fresnel relation depending on the extinction coefficient K and reflectance R as follows [24]:

$$n = \frac{(1+R)}{(1-R)} - \left(\frac{4R}{(1-R)^2} - K^2\right)^{\frac{1}{2}}. \tag{9}$$

The variation of the refractive index n of the sprayed Cu_2NiSnS_4 thin films with the wavelength was represented in Fig. 6b. It is obvious from this plot that he refractive index of the sprayed Cu_2NiSnS_4 films was increased with increasing the film thickness and decreased with the increase in wavelength λ.

3.3 Optoelectrical characterization

3.3.1 Dielectric constants

The dielectric constants of the Cu_2NiSnS_4 thin films can be determined according to the following expressions [25, 26]:

$$\varepsilon_1 = \mathrm{n}^2 - \mathrm{k}^2 \tag{10}$$

$$\varepsilon_2 = 2\mathrm{nk} \tag{11}$$

where ε_2 represents the imaginary part of the dielectric constant and the ε_1 represents the real part of dielectric constant for the Cu_2NiSnS_4 thin films.

Figure 7 a and b represents the wavelength dependence of real and imaginary part of the dielectric constant for the Cu_2NiSnS_4 films. It has been observed that the real and imaginary part of dielectric constant were increased with increasing the thickness of the Cu_2NiSnS_4 films and decreases with increasing the wavelength.

3.3.2 Optical carrier concentration and relaxation time

The ratio of the charge carrier concentrations to the effective mass, N_{opt}/m^* and the lattice dielectric constant, ε_L, of the sprayed Cu_2NiSnS_4 films have been evaluated using the presented expression [27, 28]:

$$n^2 = \varepsilon_L - \left(\frac{e^2}{4\pi^2 c^2 \varepsilon_0}\right)\left(\frac{N_{opt}}{m^*}\right)\lambda^2 \tag{12}$$

where c represents the velocity of light, e represents the electronic charge.

Figure 8 displays the dependence of n^2 on λ^2 for Cu_2NiSnS_4 thin films. The values of the N_{opt}/m^* for the Cu_2NiSnS_4 thin films were estimated from the slopes of the graph while the values of ε_L for the Cu_2NiSnS_4 thin films were evaluated from the intercept. The values of ε_L &

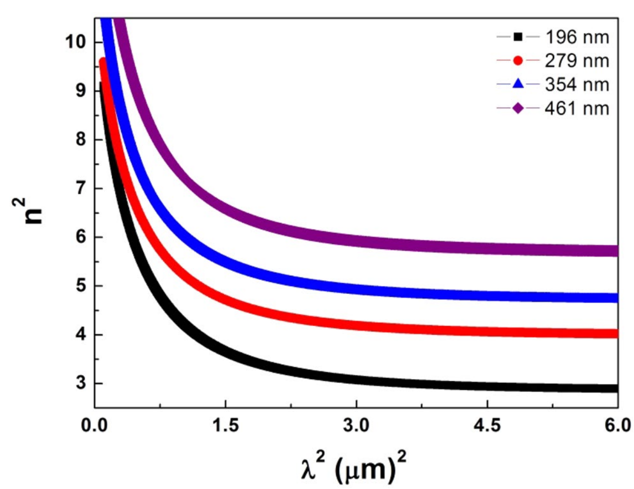

Fig. 8 The plot of n^2 versus λ^2 for the Cu_2NiSnS_4 thin films

N_{opt}/m^* estimated via this curves were recorded in Table 2. The obtained values of ε_L & N_{opt}/m^* were found to increase with increasing the Cu_2NiSnS_4 film thickness. Moreover, the magnitude of the free carrier concentration N_{opt} the sprayed Cu_2NiSnS_4 films was estimated by knowledge the value of the effective mass of the free carriers by Shen et al. [29, 30]. relation $m^* = 0.44m_0$. The values of N_{opt} were increased with the increase in film thickness.

The relaxation time, τ, of the Cu_2NiSnS_4 thin films was evaluated by the slope of the plot of the ε_2 versus λ^3 according to the presented relationship [31, 32]:

$$\varepsilon_2 = \frac{1}{4\pi^3\varepsilon_0}\left(\frac{e^2}{c^3}\right)\left(\frac{N_{opt}}{m^*}\right)\left(\frac{1}{\tau}\right)\lambda^3 \quad (13)$$

Figure 9 shows the dependence of imaginary dielectric constant ε_2 on λ^3 for the Cu_2NiSnS_4 films. The relaxation times, τ, of the Cu_2NiSnS_4 thin films was evaluated from the slope of the linear plot and was decreased with increasing the film thickness.

3.3.3 Optical mobility and optical resistivity

The optical mobility μ_{opt} and the optical resistivity ρ_{opt} of the Cu_2NiSnS_4 thin films were evaluated according to the below formulas [33–35]:

$$\mu_{opt} = \frac{e\tau}{m^*} \quad (14)$$

$$\rho_{opt} = \frac{1}{e}\mu_{opt}N_{opt} \quad (15)$$

The evaluated values for the optical mobility μ_{opt} and the optical resistivity ρ_{opt} for the Cu_2NiSnS_4 thin films were listed in Table 2. It was found that the optical mobility μ_{opt} and the optical resistivity ρ_{opt} were decreased with increasing the film thickness. This behavior agrees with other previous published data [36, 37]

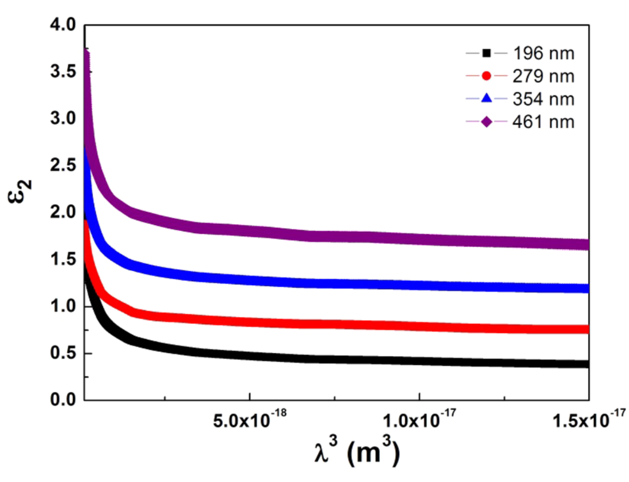

Fig. 9 The variation of the imaginary dielectric constant as a function of λ^3 for the Cu_2NiSnS_4 thin films

3.3.4 Optical and electrical conductivity evaluation

Optical conductivity (σ) means the conductance of charge carriers in material due to the optical excitation [38]. The value of optical conductivity depends on the strength of irradiation light. The optical conductivity of the Cu_2NiSnS_4 thin films has been evaluated by below formula [39]:

$$\sigma_{opt} = \frac{\alpha nc}{4\pi} \quad (16)$$

Figure 10a illustrates the variation of optical conductivity with the photon energy for the sprayed Cu_2NiSnS_4 thin films. It is observed from this plot that the optical conductivity increases with increasing the thickness and the photon energy; this behaviour attributed to the increase of electrons excitation via the increase of the incident photon energy.

The electrical conductivity of the sprayed Cu_2NiSnS_4 thin films has been estimated from the absorption coefficient, α and the optical conductivity σ_{opt} via the presented expression [40]:

$$\sigma_e = \frac{2\lambda\sigma_{opt}}{\alpha}. \quad (17)$$

The variation of the electrical conductivity with the photon energy for the Cu_2NiSnS_4 films was illustrated in Fig. 10b. It is observed from this plot that the magnitudes of the electrical conductivity for the Cu_2NiSnS_4 thin films increases with increasing the thickness and decreases with increasing the photon energy.

3.4 Nonlinear optical characterization

The evaluation of the nonlinear optical constants of the thin film like third-order nonlinear susceptibility $\chi^{(3)}$ and nonlinear refractive index n_2 is important for several applications like the large capacity communications and optical switching devices. The $\chi^{(3)}$ of the Cu_2NiSnS_4 films were calculated by the below expression [41]:

$$\chi^{(3)} = B\left[\frac{n_0^2 - 1}{4\pi}\right]^4 \quad (18)$$

where n_0 represents the values of the static refractive index, B represents a constant factor equal 1.7×10^{-10} esu.

The nonlinear refractive index n_2 of the Cu_2NiSnS_4 thin films has been calculated using the presented formula [42]:

$$n_2 = \frac{12\pi\chi^{(3)}}{n_0} \quad (19)$$

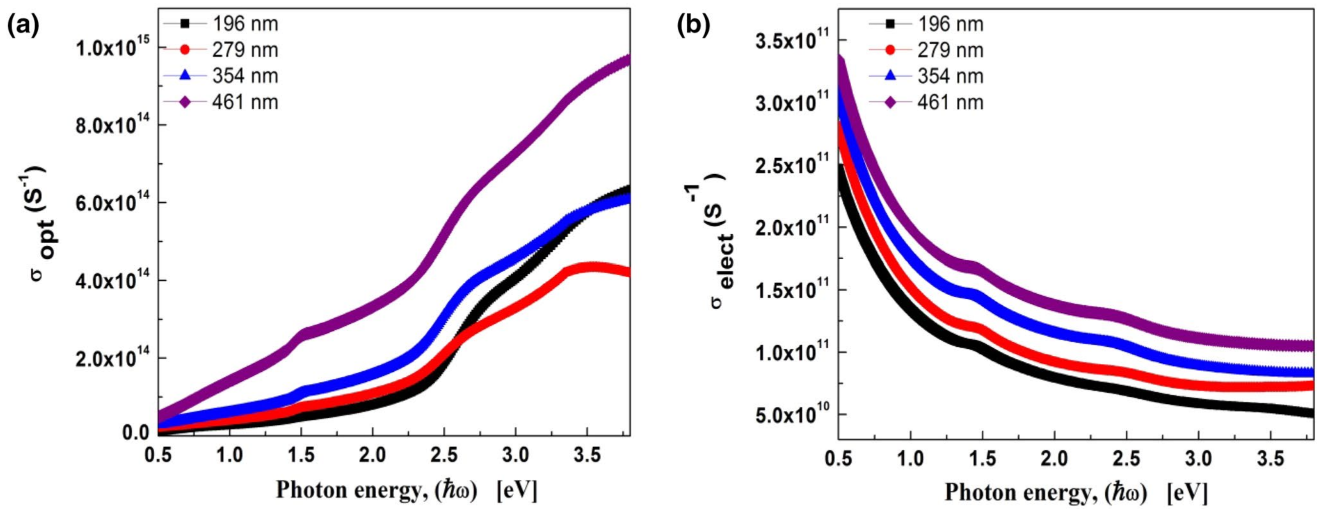

Fig. 10 **a** The dependence of the optical conductivity on the photon energy of the Cu_2NiSnS_4 thin films, **b** the electrical conductivity as a function of photon energy for the Cu_2NiSnS_4 thin film

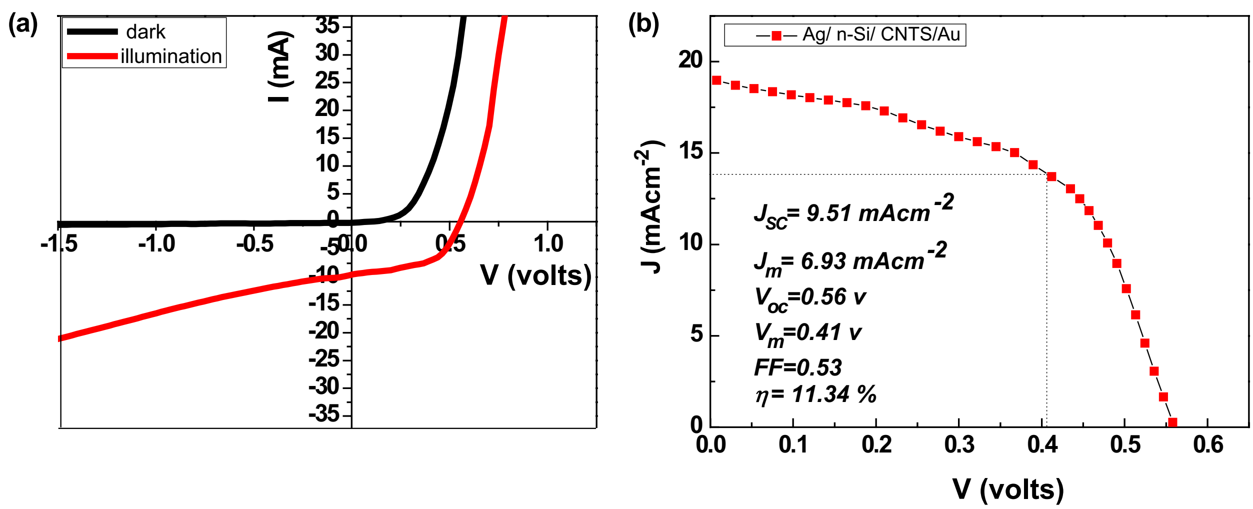

Fig. 11 **a** The I–V characteristics of the Ag/n-Si/CNSS/Au heterojunction device in dark and under illumination, **b** J–V characteristics for Ag/n-Si/CNSS/Au heterojunction under illumination of 100 mW/cm^2

The magnitudes of both $\chi^{(3)}$ and n_2 for the Cu_2NiSnS_4 thin films were listed in Table 2. It can be noticed that both parameters were found to increase with increasing the film thickness.

3.5 Photovoltaic properties of the CNSS thin films

The photovoltaic properties have been determined by measuring the dark and illuminated current–voltage (I–V) characteristics for the Ag/n-Si/CNSS/Au heterojunction. Figure 11a illustrates the I-V characteristics of the Ag/n-Si/CNSS/Au heterojunction in the dark and illumination conditions. It is observed from figure that the value of current for CNSS/n-Si heterojunction under illumination is more than the value of current in the dark. This attributed to the light absorbed produces carrier-contributing photocurrent due to the production of electron–hole pairs [43]. Figure 11b displays the J–V plot of Ag/n-Si/CNSS/Au heterojunction with area 0.5 × 0.5 cm^2 under illumination of 100 mW/cm^2.

The solar efficiency (η) of the CNSS/n-Si heterojunction can be evaluated via the following formula [44]:

$$\eta = \frac{P_{max}}{P_{in}} = \frac{FF \times V_{oc} \times J_{sc}}{P_{in}} \times 100\%, \quad (20)$$

where P_{in} is the input energy from the sun and P_{max} is the output energy from the solar cell.

The device parameters estimated for Ag/n-Si/CNSS/Au heterojunction are V_{OC}= 0.56 V, J_{SC}= 18.96 mAcm^{-2}, V_m= 0.41 V, J_m= 13.83 mAcm^{-2}, FF = 0.53 and efficiency = 11.34%.

4 Conclusion

In this study, spray pyrolysis technique was utilized to deposit Cu_2NiSnS_4 thin films at different thickness (196, 279, 354 and 461 nm). The XRD analysis of the Cu_2NiSnS_4 films displays that the as-deposited Cu_2NiSnS_4 thin films are polycrystalline with a cubic structure. The linear optical properties of the Cu_2NiSnS_4 thin films have been studied in the spectral range 400-2500 nm. The refractive index of the Cu_2NiSnS_4 films was found to increase with increasing the thickness. The type of optical transition in the Cu_2NiSnS_4 thin films was detected to be direct allowed transition. The optoelectrical parameters of the Cu_2NiSnS_4 films, like optical conductivity, optical mobility, optical resistivity, optical carrier concentration, electrical conductivity and relaxation time were evaluated. The effect of thickness on the non-linear optical parameters has been studied. The Ag/n-Si/CNSS/Au heterojunction has been fabricated using the CNSS film of thickness 461 nm. This device has a solar conversion efficiency of 11.34%.

References

1. S. Siebentritt, S. Schorr, Kesterites—a challenging material for solar cells. Prog. Photovolt. **20**(5), 512–519 (2012)
2. M. Nakashima, T. Yamaguchi, S. Yukawa, J. Sasano, M. Izaki, Effect of annealing on the morphology and compositions of $Cu_2ZnSnSe_4$ thin films fabricated by thermal evaporation for solar cells. Thin Solid Films **621**, 47–51 (2017)
3. A. Walsh, S. Chen, S.-H. Wei, X.-G. Gong, Kesterite thin-film solar cells: advances in materials modelling of Cu2ZnSnS4. Adv. Energy Mater. **2**(4), 400–409 (2012)
4. S.S. Fouad, I.M. El Radaf, P. Sharma, M.S. El-Bana, Multifunctional CZTS thin films: structural, optoelectrical, electrical and photovoltaic properties. J. Alloys Compds. **757**, 124–133 (2018)
5. A. Ennaoui, M. Lux-Steiner, A. Weber, D. Abou-Ras, I. Kötschau, H.-W. Schock, R. Schurr, A. Hölzing, S. Jost, R. Hock, Cu_2ZnSnS_4 thin film solar cells from electroplated precursors: novel low-cost perspective. Thin Solid Films **517**(7), 2511–2514 (2009)
6. X. Zeng, K.F. Tai, T. Zhang, C.W.J. Ho, X. Chen, A. Huan, T.C. Sum, L.H. Wong, Cu2ZnSn(S, Se)4 kesterite solar cell with 5.1% efficiency using spray pyrolysis of aqueous precursor solution followed by selenization. Solar Energy Mater. Sol. Cells **124**, 55–60 (2014)
7. M.S. Kumar, S.P. Madhusudanan, S.K. Batabyal, Substitution of Zn in Earth Abundant Cu2ZnSn(S, Se)4 based thin film solar cells—a status review. Sol. Energy Mater. Sol. Cells **185**, 287–299 (2018)
8. A. Jariwala, T.K. Chaudhuri, S.P.A. Toshniwal, V. Kheraj, A. Ray, Direct-coated copper nickel tin sulphide (Cu_2NiSnS_4) thin films from molecular ink. Mater. Lett. **215**, 118–120 (2018)
9. T.-X. Wang, Y.-G. Li, H.-R. Liu, H. Li, S.-X. Chen, Flower-like Cu_2NiSnS_4 nanoparticles synthesized by a facile solvothermal method. Mater. Lett. **124**, 148–150 (2014)
10. S. Sarkar, B. Das, P.R. Midya, G.C. Das, K.K. Chattopadhyay, Optical and thermoelectric properties of chalcogenide based Cu_2NiSnS_4 nanoparticles synthesized by a novel hydrothermal route. Mater. Lett. **152**, 155–158 (2015)
11. A. Kamble, K. Mokurala, A. Gupta, S. Mallick, P. Bhargava, Synthesis of Cu_2NiSnS_4 nanoparticles by hot injection method for photovoltaic applications. Mater. Lett. **137**, 440–443 (2014)
12. A. Ghosh, A. Biswas, R. Thangavel, G. Udayabhanu, Photo-electrochemical property and electronic band structure of kesterite copper chalcogenides Cu2-II-Sn-S4 (II = Fe Co, Ni) thin films. RSC Adv. **6**, 96025–96034 (2016)
13. H.-J. Chen, S.-W. Fu, T.-C. Tsai, C.-F. Shih, Quaternary Cu_2NiSnS_4 thin films as a solar material prepared through electrodeposition. Mater. Lett. **166**, 215–218 (2016)
14. K. Mokurala, S. Mallick, P. Bhargava, S. Siol, T.R. Klein, M.F.A.M. van Hest, Influence of dipping cycles on physical, optical, and electrical properties of Cu_2NiSnS_4: direct solution dip coating for photovoltaic applications. J. Alloys Compds. **725**, 510–518 (2017)
15. A.L. Patterson, The Scherrer formula for X-ray particle size determination. Phys. Rev. **56**, 978 (1939)
16. A.Y. Shenouda, M.M. Rashad, L. Chow, Synthesis, characterization and performance of $Cd_{1-x}In_xTe$ compound for solar cell applications. J. Alloys Compds. **563**, 39–43 (2013)
17. T.A. Hameed, I.M. El Radaf, H.E. Elsayed-Ali, Characterization of $CuInGeSe_4$ thin films and Al/n–Si/p–$CuInGeSe_4$/Au heterojunction device. J. Mater. Sci. **29**, 12584–12594 (2018)
18. Xu Wang, Tilantlan Liu, Hao Guan, Yu. Fangli, Haijun Hou, A comparative study of Cu_2MnSnS_4 thin films synthesized via different chemical methods. J. Optoelectron. Adv. Mater. **9**, 1190–1193 (2015)
19. I.M. El Radaf, S.S. Fouad, A.M. Ismail, G.B. Sakr, Influence of Spray time on the optical and electrical properties of $CoNi_2S_4$ thin films. J. Mater. Res. Express **5**, 046406 (2018)
20. M.S. El-Bana, R. Bohdan, S.S. Fouad, Optical characteristics and holographic gratings recording on $As_{30}Se_{70}$ thin films. J. Alloy. Compd. **686**, 115–121 (2016)
21. J. Tauc, R. Grigorovici, A. Vancu, Optical properties and electronic structure of amorphous germanium. Phys. Status Solidi (B) **15**, 627–637 (1966)
22. I.S. Yahia, I.M. El Radaf, A.M. Salem, G.B. Sak, Chemically deposited Ni-doped CdS nanostructured thin films: optical analysis and current-voltage characteristics. J. Alloy. Compd. **776**, 1056–1062 (2019)
23. T.A. Hameed, I.M. El Radaf, G.B. Sakr, Synthesis and characterization of thermochromic Ag2HgI4 thin flms. Appl. Phys. A **124**, 684 (2018)
24. M.S. El-Bana, G. Mohammed, A.M. El Sayed, S. El-Gamal, Preparation and characterization of PbO/carboxymethyl cellulose/polyvinylpyrrolidone nanocomposite films. Polym. Compos. **39**, 3712–3725 (2017)
25. M. Fadela, I.S. Yahia, G.B. Sak, F. Yakuphanoglu, S.S. Shenouda, Structure, optical spectroscopy and dispersion parameters of $ZnGa_2Se_4$ thin films at different annealing temperatures. Opt. Commun. **285**, 3154–3161 (2012)
26. I.M. El Radaf, R.M. Abdelhameed, Surprising performance of graphene oxide/tin dioxide composite thin films. J. Alloy. Compd. **765**, 1174–1183 (2018)
27. M.S. El-Bana, I.M. El Radaf, S.S. Fouad, G.B. Sakr, Structural and optoelectrical properties of nanostructured $LiNiO_2$ thin films

grown by spray pyrolysis technique. J. Alloy. Compd. **705**, 333–339 (2017)
28. P. Sharma, M.S. El-Bana, S.S. Fouad, V. Sharma, Effect of compositional dependence on physical and optical parameters of $Te_{17}Se_{83-x}Bi_x$ glassy system. J. Alloy. Compd. **667**, 204–210 (2016)
29. Q. Shen, K. Katayama, T. Sawada, T. Toyoda, Characterization of electron transfer from CdSe quantum dots to nanostructured TiO_2 electrode using a near-field heterodyne transient grating technique. Thin Solid Films **516**, 5927–5930 (2008)
30. Q. Shen, T. Toyoda, Characterization of nanostructured TiO_2 electrodes sensitized with CdSe quantum dots using photoacoustic and photoelectrochemical current methods. Jpn. J. Appl. Phys. **43**, 2946 (2004)
31. A.S. Hassanien, Studies on dielectric properties, opto-electrical parameters and electronic polarizability of thermally evaporated amorphous $Cd_{50}S_{50-x}Se_x$ thin films. J. Alloy. Compd. **671**, 566–578 (2016)
32. A. Hassanien, A.A. Akl, Influence of composition on optical and dispersion parameters of thermally evaporated non-crystalline Cd 50 S 50–x Se x thin films. J. Alloy. Compd. **648**, 280–290 (2015)
33. M.S. El-Bana, R. Bohdan, S.S. Fouad, Optical characteristics and holographic gratings recording on $As_{30}Se_{70}$ thin films. J. Alloy. Compd. **686**, 115–121 (2016)
34. M.S. El-Bana, S.S. Fouad, Opto-electrical characterisation of $As_{33}Se_{67-x}Sn_x$ thin films. J. Alloy. Compd. **695**, 1532–1538 (2017)
35. P. Sharma, M.S. El-Bana, S.S. Fouad, V. Sharma, Effect of compositional dependence on physical and optical parameters of $Te_{17}Se_{83-x}Bi_x$ glassy system. J. Alloy. Compd. **667**, 204–210 (2016)
36. S.S. Fouad, E.A.A. El-Shazly, M.R. Balboul, S.A. Fayek, M.S. El-Bana, Optical parameter studies of thermally evaporated As-Se-Sn glassy system. J. Mater. Sci. **17**, 193–198 (2006)
37. S.S. Fouad, M.S. El-Bana, P. Sharma, V. Sharma, Analysis of chemical ordering and fragility for Ge–Se–In glasses. Appl. Phys. A **120**, 137–143 (2015)
38. S. Gedi, V.R.M. Reddy, C. Park, J. Chan-Wook, K.T.R. Reddy, Comprehensive optical studies on SnS layers synthesized by chemical bath deposition. Opt. Mater. **42**, 468–475 (2015)
39. G.B. Sakr, I.S. Yahia, M. Fadel, S.S. Fouad, N. Romčević, Optical spectroscopy, optical conductivity, dielectric properties and new methods for determining the gap states of CuSe thin films. J. Alloy. Compd. **507**, 557–562 (2010)
40. M. El-Mansy, M. El-Bana, S. Fouad, On the spectroscopic analyses of 3-hydroxy-1-phenyl-pyridazin-6 (2H) one (HPHP): a comparative experimental and computational study. Spectrochim. Acta, Part A **176**, 99–105 (2017)
41. I.M. El Radaf, T.A. Hamid, I.S. Yahia, Synthesis and characterization of F-doped CdS thin films by spray pyrolysis for photovoltaic applications. J. Mater. Res. Express **5**, 066416 (2018)
42. R.M. Abdelhameed, I.M. El Radaf, Self-cleaning lanthanum doped cadmium sulfide thin films and linear/nonlinear optical properties. J. Mater. Res. Express **5**, 066402 (2018)
43. I.M. El Radaf, M.S. Al-Kotb, M. Nasr, I.S. Yahia, Fabrication and electrical characterization of the $InSbS_3$/n-Si heterojunction. J. Alloy. Compd. **788**, 206–211 (2019)
44. M. Nasr, I.M. El Radaf, A.M. Mansour, Current transport and capacitance–voltage characteristics of an n-PbTe/p-GaP heterojunction prepared using the electron beam deposition technique. J. Phys. Chem. Solids **115**, 283–288 (2018)